Engineering and Technology Journal
Journal homepage: https://etj.uotechnology.edu.iq

Moment-curvature relations of fiber-reinforced concrete-encased CFST beams

Raad Abdulkhudhur*, Hussein Al-Quraishi, Mohammed Elwi

Civil Engineering Dept., University of Technology-Iraq, Alsina'a street, 10066 Baghdad, Iraq.
*Corresponding author Email: raad.a.sehaib@uotechnology.edu.iq

HIGHLIGHTS

- The study examined nine concrete-encased CFST beams with varying section sizes, CFST ratios, and steel fibers
- The ultimate moment and curvature of CFST beam were 41% and 328.95% of that conventional beam
- Increasing section height, CFST ratio, and concrete strengths enhanced the ultimate moment, while unfilled tubes reduced it

Keywords:

Moment-curvature relations
CFST beams
Steel fiber content
Four-point load test
Modes of failure

ABSTRACT

A concrete-filled steel tube surrounded by external concrete is a composite element known as a concrete-encased concrete-filled steel tube (CFST). This composite element is used in multi-story buildings, large-span constructions, bridges, and underground transit stations. This research examined the curvature behavior of fiber-reinforced concrete-encased CFST beams. Eight concrete-encased CFST beams and one conventional beam were subjected to four-point loads during testing. The factors examined were shear connection, section size, CFST ratio, outer concrete compressive strength, compressive strength of concrete inside the steel tube, steel fiber content, and unfilled steel tubes. Curvature is an important factor that determines the adequacy of reinforced concrete beams because it depends on the deflections, which are considered the major factor for accepting or rejecting the structural members in buildings. The test results showed that the conventional beam's ultimate moment is 141.9% greater than that of the concrete-encased CFST. Also, the curvature of the conventional beam is 30.4% lower than that of a reference beam constructed from concrete-encased CFST. Furthermore, increasing the CFST ratio from 2.7% to 5.4% resulted in a 62.4% enhancement in the ultimate moment, accompanied by an 11.3% reduction in beam curvature. Increasing the outer compressive strength of concrete from 25 MPa to 45 MPa resulted in a 13.8% rise in the ultimate moment and a 19.03% reduction in the beam's curvature. When the compressive strength of the concrete inside the inner steel tubes was raised from 35 MPa to 55 MPa, the ultimate moment went up by 6.7%, and the beam's curvature went down by 11.3% compared to the reference beam. The absence of steel fiber in concrete-encased CFST reduces the ultimate moment by 6.1% and diminishes the curvature by 22.3%. The unfilled steel tube inside concrete-encased CFST reduces the ultimate moment by 13.97%, while the curvature rises by 3.6%. The results show that section size, CFST ratio, outer concrete compressive strength, shear connection, and compressive strength of concrete inside the steel tube are the best results. In contrast, steel fiber content and unfilled steel tubes have the worst results compared to the reference beam.

1. Introduction

A composite construction consists of a concrete-filled steel tube (CFST) component, which is covered in an exterior concrete layer. The ductility of concrete-encased CFST surpasses that of traditional reinforced concrete elements [1-3]. Concrete-encased CFSTs are increasingly used in the construction of edifices and bridges due to their superior mechanical properties [1,4]. When a concrete-encased CFST box element is used as an arch or pier, it mostly undergoes axial compression or a combination of axial compression and bending [5,6]. Concrete-encased CFST box members, although seldom subjected to pure bending, exhibit considerable bending strength and stiffness, making them appropriate for use as bridge girders. Pure bending denotes the most severe condition of beam-column behavior, marked by the lack of any axial stress [6,7]. Previous research has explored the behavior of concrete-encased concrete-filled steel tube (CFST) components under bending.

http://doi.org/10.30684/etj.2025.155767.1865
Received 12 December 2024; Received in revised form 23 January 2025; Accepted 01 March 2025; Available online 03 June 2025
2412-0758/University of Technology-Iraq, Baghdad, Iraq

Y-F et al. [8], analyzed the flexural performance of these components using numerical methods. A finite-element analysis (FEA) model is developed to examine the bending characteristics of the composite part, and empirical evidence corroborates it. The relationship between moment and curvature, stress distributions in composite sections, and interactions between steel and concrete were thoroughly investigated. The parametric analysis presents simplified equations to predict the flexural strength of concrete-encased CFST sections.

Han et al. [9], conducted a study where they tested and used finite element analysis (FEA) on numerous large concrete-encased concrete-filled steel tube (CFST) box members. The investigation included testing two reinforced concrete (RC) box members and six concrete-encased CFST box members. The study looked at how different steel tube diameters (74.9 mm to 102.2 mm) and sectional heights (840 mm to 1260 mm) affected the ability of concrete-encased CFST box members to bend. A comparative analysis of the failure processes and performance of concrete-encased CFST box members vs. similar RC box members under bending was conducted. Finite Element Analysis (FEA) was used to investigate the bending of concrete-encased Concrete-Filled Steel Tubes (CFST) box members. Conducted an extensive analysis of the moment-curvature relationship, load transfer mechanisms, and the shear-span-to-depth ratio. Recent research by Chen et al. [10], investigated the performance of twelve concrete-encased CFST box beams. The research sought to evaluate the influence of section size, steel tube diameter, and bending direction on the performance of beams. The test results were examined, including the identified failure patterns and the formation of concrete fractures throughout the whole loading process. Montuori and Piluso [11], evaluated concrete-filled tubular (CFT) members' ultimate behavior under non-uniform bending forces. Eight Square Hollow Section (SHS) CFT members were tested under monotonic loading. In the three-point bending technique for testing specimens, a hydraulic actuator applies the transverse load at midspan while controlling the displacement. An LVDT measures the largest transverse displacement. Strain gauges were used to quantify longitudinal deformations across the cross-section perimeter to analyze the moment-curvature relationship experimentally. Li et al. [12], tested six specimens with different steel ratios of high-strength concrete-filled square steel tubes (HCFHST) under pure bending stresses. Mechanical properties were examined using nonlinear finite-element models. The computed load-displacement curves match the experimental results. The moment-curvature relationship has elastic, yield, and hardening phases. Steel ratio, yield strength, and concrete compressive strength improve ultimate bearing capacity. Hou et al. [13], used experimental and computational approaches to study the lateral impact behavior of CFST box beams and columns. Twenty samples were drop-hammer tested. Impact energy, boundary conditions, and axial load were tested. Experimental findings are analyzed for failure mechanisms, impact force time history, mid-span deflection, and impact process. Impact findings show shear-flexural failure in the specimens. A study summarizes impact force and mid-span deflection curve parameters. The research also addresses how the specimens' peak impact force, impact duration, and residual mid-span deflection are affected. The combined impacts of RC and CFST components are studied using an FEM model. According to the investigation, the RC component greatly increases the structure's impact resistance. The RC component protects the CFST components, preventing major damage. The effects improve structural safety during impact loading and post-impact repair.

Chen et al. [14], used twelve concrete-encased CFST box beams to investigate their performance. The research examined how section size, steel tube diameter, and bending direction affect beam performance. Failure patterns and concrete fractures with loading were investigated. A computer model was then constructed to examine composite beam flexural properties. All parameters, including load transfer mechanisms and stress distribution, were examined. Further parametric investigations used FEA modeling. This work developed a technique to estimate concrete-encased CFST box beam stiffness and flexural strength. Based on the limited investigation, the study concludes:

(1) All specimens failed flexural. Outside reinforced concrete (RC) was severely damaged in the top portion, but the inner concrete-filled steel tube (CFST) was generally uninjured in the center. The pure bending zone has equally distributed flexural fractures. As the inner CFST diameter (D) increased, vertical concrete fracture width (w) decreased. Meanwhile, ultimate moment (Mu) grew from 27.6% to 30.3%.

(2) Flexural behavior was extensively analyzed using the verified FEA model. Five phases were identified in the M-ϕ connection during the loading history. The RC component attained load-carrying capacity, whereas the CFST components reached 82% of their maximal strength at ϕ_u. Reinforced Concrete (RC) and Concrete-Filled Steel Tube (CFST) components caused stress redistribution during descent. The popular strut-tie model described load transmission using stress distributions.

(3) A parametric study showed that MU increased with higher values of f_{ys}, α_s, f_{yl}, $f_{cu,out}$, and α_l. However, $f_{cu,out}$did not affect MU. Increases in f_{ys}, α_s, f_{yl}, and α_l may increase residual moment. Initial stiffness and final bending capacity were predicted using simpler methods.

Al Zand et al. [15], came up with new empirical ways to accurately predict the bending moment capacity (Mu) and flexural stiffness of composite beams made of concrete-filled steel tubes at both the initial and serviceability levels. These empirical methodologies need a wide collection of Mu, Ki, and Ks data, including CFST beam parameters. Thus, finite element software was used to create 144 numerical CFST models. Comparing recently developed empirical approaches to earlier experimental and numerical studies by other experts verified their efficacy. Comparing projected Mu values to published values for square and round CFST beams yielded average values of 0.967 and 0.996, respectively, using the new approaches. The average anticipated Ki and Ks values were 1.074 and 1.050. Al Zand et al. [16], investigated the flexural behavior of a slender steel tube beam. This beam was constructed by joining two C-sections and filling them with recycled aggregate concrete, resulting in a CFST beam. The lips of the C-section functioned as internal stiffeners for the cross-section of the CFST beam. A flexural test was conducted on five large-scale specimens, including one hollow specimen devoid of concrete material. The ABAQUS software facilitated the simulation and analysis of an additional 20 CFST models. This was conducted to investigate the effects of various parameters that were not examined in the experiments. The numerical model correctly predicted the tested specimen's flexural behavior and failure mode, though it was slightly off by about 3.1% when it came to the flexural strength capacity. The research validated the efficacy of employing tubular C-sections within the CFST beam framework. The incorporation of internal

stiffeners, or lips, led to significant improvements in flexural strength, stiffness, and energy absorption index. A novel analytical technique was developed to predict the flexural strength capacity of internally accurately stiffened CFST beams with steel stiffeners. Liu et al. [17], conducted a four-point bending study on ten rectangular HSFRC-filled steel tubular (HSFRCFST) beams, which were filled with HSFRC. Most important were HSFRC strength grade, steel fiber content, internal stiffener type, and perfobond stiffener circular hole spacing. Moment curvature and flexural load-deflection curves were calculated. Crack dispersion and infill HSFRC failure mode were found. The findings revealed that a 1.2% volume of steel fibers enhanced HSFRCFST beam bending stiffness and moment capacity. Tests show that using the right steel fiber mix and perfobond stiffener spacing between round holes can make rectangular HSFRCFST beams much less likely to bend. In construction, parameter designs may increase steel fiber-reinforced concrete beam ductility and bearing capacity. Last, a rectangular HSFRCFST beam design formula with stiffeners' moment capacity fits experimental findings. Suthar et al. [18], studied the moment-curvature of reinforced concrete beams, whose performance depends on their capacity to endure substantial inelastic deformation. To conduct nonlinear analysis, techniques like pushover analysis need inputs like critical section moment-curvature relationships. Analytical and experimental research on RC rectangular statically determinate beam sections is proposed. Flexural testing was done on beams. Concrete and steel behavior was recorded. Experimental validation was conducted using confinement models from several research articles. Suresh and Mohamed [19], analyzed beam moment-curvature sections using MC-BAM. This tool aids in the study and structural design of beams and girders using sophisticated materials such as UHPC, high-strength steel rebars, and massive prestressing strands. MCBAM supports rectangular, circular, and other cross-sections like I- or Pi-girders using numerous current, newly developed, or user-defined constitutive material models. The material models and section analysis technique are validated for ordinary materials using commercial software and textbook examples and subsequently for advanced materials and designs using published experimental data. Al-Thairy's study [20], shows that one of the most frightening events that could potentially lead to the collapse and failure of steel structures is fire. Current design guidelines and standards include fire as an extreme loading condition for structures. Many of these regulations and standards' methods are inaccurate and illogical. This work proposes an analytical method to forecast the elastic-plastic moment-curvature connection of steel beam-column sections at high temperatures. The analytical method was derived by dividing the steel section into layers and integrating the resistance moment equation of each layer in terms of section curvature, taking into account the effect of elevated temperature on steel material properties by using EC3 yield stress and modulus of elasticity reduction factors. Numerical simulations verified the proposed strategy. The validation results show that the suggested method can accurately predict the resistance moment-curvature relationship of steel beam-column members when exposed to a range of high temperatures and axial compressive forces. The recommended strategies may improve the design of fire-resistant steel beam-columns. Fa-xing and Zhi-wu [21], used a layered technique to examine the full moment-curvature curves of concrete-filled circular steel tubes (CFST) subjected to pure bending using the appropriate numerical constitutive model. The tests of three self-compacting concrete-filled circular steel tubes and one normal concrete-filled circular steel tube subjected to pure bending were conducted, and the effects of concrete strength and steel ratio on the specimens' pure bending properties were discussed. Experimental results show that the confinement effect between the steel tube and concrete occurs on the compressive side. Still, the steel tube is in biaxial tensile stress conditions on the tensile side. As concrete strength increases, specimen flexural capacities are slightly affected, but the increase in steel ratio improves them. Wu et al. [22], tested four rubber concrete-filled steel tube (RuCFST) members, one CFST member, and one empty member under pure bending. The key parameters were a 3 to 5 shear span ratio (λ) and a 10% to 20% rubber replacement ratio (r). The study obtained the bending moment-strain, deflection, and curvature curves. The failure mechanisms of core rubber concrete were examined. Results showed bending failure in RuCFST members. Rubber concrete fissures were infrequent and uniformly distributed, while rubber infill in core concrete prevented cracks. The shear span ratio has minimal influence on specimen behavior. The studied specimens' bending stiffness was affected by the rubber replacement ratio but not the bending moment capacity. Rubber concrete improves bending moment capacity and stiffness compared to empty steel tubes. Rahmani et al. [23], found that concrete-encased concrete-filled tubes contain faults owing to their poor tensile strength. Concrete-filled tubes (CFTs) and prestressing strands enclosed in concrete were combined using an acceptable approach. Sections using high-strength materials need more examination since typical design principles are intended for normal-strength materials. This study used high-strength concrete and steel to study the impact on core confinement, sectional size, and flexural behavior of high-strength prestressed concrete-encased concrete-filled steel tube (HS-PCE-CFST) beams while developing the design process. The ABAQUS finite element software modeled thirteen HS-PCE-CFST beams. Key factors are steel tube yield strength, core and outside concrete compressive cylinder strength, and steel tube diameter to section width ratio. Experimental findings were used to validate the finite element model. It also analyzes the bending moment, ductility, flexural stiffness, and failure mechanism of beams. Results indicate that outer concrete compressive strength has the greatest impact on flexural parameters. Increasing the ratio of steel tube diameter to section width leads to a minor increase in ultimate bending moment and serviceability level flexural stiffness but a significant increase in initial stiffness. Hamoda et al. [24], examined reinforced concrete (RC) circular column structural performance under double curvature buckling moment experimentally and computationally. RC circular columns are popular in RC constructions for their aesthetics, ease of construction, and stress tolerance. Corner or edge columns may experience edge moment (EM) from the beam-column junction with a double curvature effect. The study examines the structural behavior of such columns under double curvature buckling edge moment at the beam-column connection using specific parameters. Eleven full-scale RC circular columns were built, mounted, and tested to failure using four parameters. The criteria included clear height-to-diameter ratio (λ), longitudinal and lateral steel ratios (μ and ρ), and concrete type. Introduced λ ratios: 4.89, 4.51, and 4.14; μ ratios: 2.2, 2.3, 2.6, and 3.1%; ρ ratios: 0.84, 0.93, 1.00, and 1.18%. Three concrete types were studied: normal concrete (NC), engineered cementitious composite (ECC), and high-strength fiber-reinforced concrete (HSFRC). Experimental results showed that all factors may improve structural performance, but longitudinal reinforcement and height-to-

diameter ratio improved performance by 51%–64%. Along with experimental results, nonlinear three-dimensional finite element models (FEMs) were installed, run, and constructed to provide an appropriate model with a 4% under/overestimation.

In summary, the majority of prior studies focus on concrete-filled steel tube beams as composite elements, while fewer studies address concrete-encased-filled steel tube members. No one has addressed the use of steel fiber to reinforce the outer concrete.

2. Experimental work

2.1 Specimens details

One conventional beam reinforced with steel bars measured 160 ×260 ×2000 mm^3, seven concrete-encased CFST beams measured 160 x 260 x 2000 mm^3, and one concrete-encased CFST beam measured 160 x 340 x 2000 mm^3, all reinforced with steel fiber and featuring a steel tube filled with self-compacted concrete. The steel tubes are welded to a 10mm diameter steel bar to inhibit slippage between the concrete and the steel tubes in concrete-encased CFST beams. Additionally, all beams undergo testing with four-point loads to assess their flexural behavior.

The experiment looked at things like section size, steel fiber content, compressive strength of the concrete on the outside, compressive strength of the concrete inside the steel tube, the presence of a shear connection, the CFST ratio (cross area of CFST over the cross-sectional area of outer concrete), and an empty steel tube. Table 1 delineates the parameters of the examined beams and the factors taken into account. The hooked-end steel fiber used in this study measures 35 mm in length and 0.6 mm in diameter, has an aspect ratio of 58 and exhibits an ultimate tensile strength of 1000 MPa. The used steel tubes have a diameter of 25 mm and a thickness of 1.8 mm, exhibiting a yield strength of 456 MPa and an ultimate tensile strength of 492 MPa. The 25 mm diameter deformed steel bars have a yield strength of 581.74 MPa and an ultimate tensile strength of 681.31 MPa. They are used as the main reinforcement at the bottom of normal beams at both the top and bottom of the cross-section. The deformed steel bars, with a diameter of 10 mm, yield strength of 555 MPa, and an ultimate tensile strength of 651.8 MPa, function as bracing to prevent slippage of the supporting steel tubes. Figure 1 illustrates the geometric size and configuration of CFSTs and bracing in the specimens.

Table 1: Experimental work and beam variables for this investigation

No.	Variable	Section size (h) (mm)	Volume fraction of steel fiber %	Compressive strength of outer concrete	Compressive strength of concrete in steel tube (MPa)	Shear connector spacing (mm)	CFST %
B1	Conventional	260	1	25	---	---	---
B2	Reference	260	1	25	35	---	2.7
B3	Presence of shear connector	260	1	25	35	75	2.7
B4	Section size	340	1	25	35	---	2.0
B5	Ratio of CFST	260	1	25	35	---	5.4
B6	Compressive strength of outer concrete	260	1	45	35	---	2.7
B7	Compressive strength of concrete in FST	260	1	25	55	---	2.7
B8	Steel fiber content	260	1	25	35	---	2.7
B9	Unfilled steel tube	260	1	25	---	---	2.7

The specimens were created using Portland cement type I, which has a specific gravity of 3.15 gm/cm^3. The study utilized a fine aggregate with a grading test that is classified as zone 2 and a natural coarse aggregate with a maximum size of (5–14) mm. The mixes used to manufacture the specimens contained silica fume with a specific gravity of 2.2 g/cm^3, which constituted 10% of the weight of cement. This study utilized viscocrete-905 with a specific gravity of 1.065 g/cm^3 as a high-range water-reducing, retarding, and slump-retaining admixture to decrease the ratio of water to cement in concrete and enhance the strength of concrete as shown in Table 2.

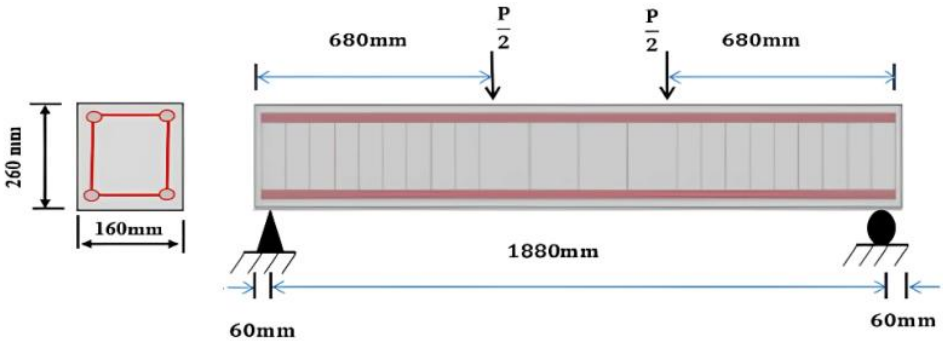

Figure 1: Concrete-encased CFST beam

2.2 Mix proportion

As shown in Table 2, the experimental mixtures are divided into two groups. The first group is meant to make self-compacting concrete-filled steel tubes with strengths of 35, 45, and 55 MPa. The second group is meant to make outer normal-strength concrete encased CFST with strengths of 25, 35, and 45 MPa.

Table 2: SCC-filled steel tube and outer concrete NC mix proportions

Mix type	Cement kg/m^3	Gravel kg/m^3	Sand kg/m^3	Silica fume kg/m^3	water kg/m^3	Water to binder ratio (w/b)	Water to binder ratio (w/c)	Steel Fiber %	Super plasticizer %	Compressive strength of cylinders MPa
SCC1	420	841	841	42	218	0.472	0.52	0	1.11	35
SCC2	520	800	800	52	200	0.35	0.38	0	1.28	45
SCC3	550	833	833	55	165	0.273	0.30	0	1.82	55
NC1	350	912	850	0	193	0.55	0.55	1%	0.95	25
NC2	460	912	770	0	200	0.43	0.43	1%	1.0	35
NC3	550	912	690	0	165	0.3	0.30	1%	1.0	45

2.3 Testing of fresh SCC

Three major tests, slump flow, L-box, and V-funnel, may be done immediately after each trial mix to determine the qualities of SCC, including filling ability, passage ability, and segregation resistance. All of these tests were carried out according to the recommendations of EFNARC (2002) [25].

2.3.1 Slump flow and (T_{500}) tests

The slump has a simple and quick method; it is used to assess the flow ability of SCC. This test examined two main aspects: filling ability by measuring the horizontal flow diameter SF and mix viscosity by measuring the time required for SCC to reach 500 mm flow (T_{500}). This test can detect segregation resistance visually. Due to its simplicity, the slump test can be performed on-site or in the laboratory using an inverted or upright Abram's cone. The cone is put on a leveled flat steel surface with a plane area of at least 900 mm by 900 mm, filled with SCC, and hoisted in 2 to 4 seconds to a height of 15 to 30 mm; the SCC mix flows out under the pull of gravity. Two horizontal perpendicular diameters, d1 and d2, as observed in Figure 2, are measured, and the average flow spread diameter SF is determined using Equation 1:

$$SF = \frac{d1+d2}{2} \quad (1)$$

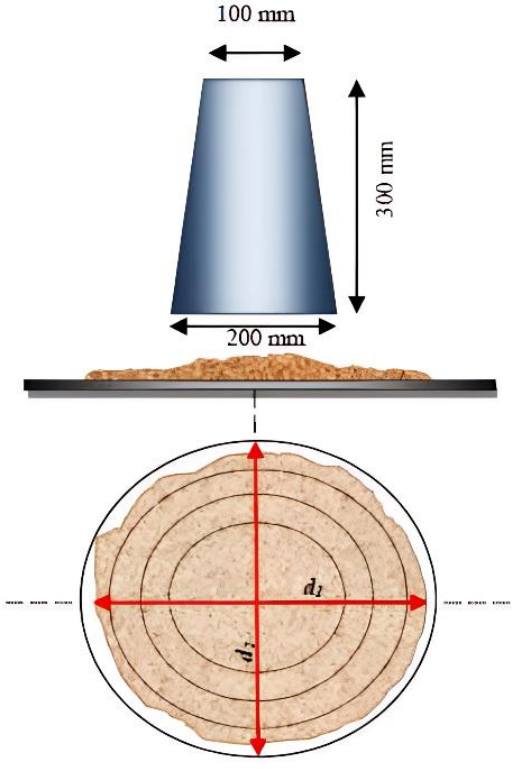

Figure 2: Slump test apparatus with cone

The slump flow test is depicted in Plate 1.

Plate 1: Slump flow test of SCC

The acceptance criteria for the slump flow test must comply with the requirements of BS EN 12350-8, 2010 [26].

- The capacity to achieve a large diameter without segregation implies good deformability and low yield stress.
- T_{500} must be noted as "the time required for SCC mix to make a diameter of 500 mm.
- This test is not acceptable when the greatest aggregate size is greater than 40 mm.
- The variation between d1 and d2 must not exceed 50 mm; otherwise, the test has to be conducted again.
- Segregation can be identified visually by evaluating a ring of cement paste or mortar at the flow's edge and/or ensuring that no coarse particles or fibers have lifted in the flow's center.

2.3.2 L-box test

The L-box test is used to assess SCC filling and passing ability, which refers to the ability of concrete to pass between reinforced bars without blocking or segregation. The L-Box is made up of two parts: a vertical part and a horizontal part separated by a hole containing three bars, as shown in Figure 3. After filling the L-box's vertical portion, the gate is lifted to allow SCC to flow into the horizontal portion after passing through the rebar impediments. Two heights of concrete are measured (H1 and H2) at the beginning and conclusion of the horizontal portion, respectively. The filling ability is shown by the H2/H1 ratio, which must normally be 0.8~1. By physically inspecting the region around the rebar, it is possible to detect the passing ability.

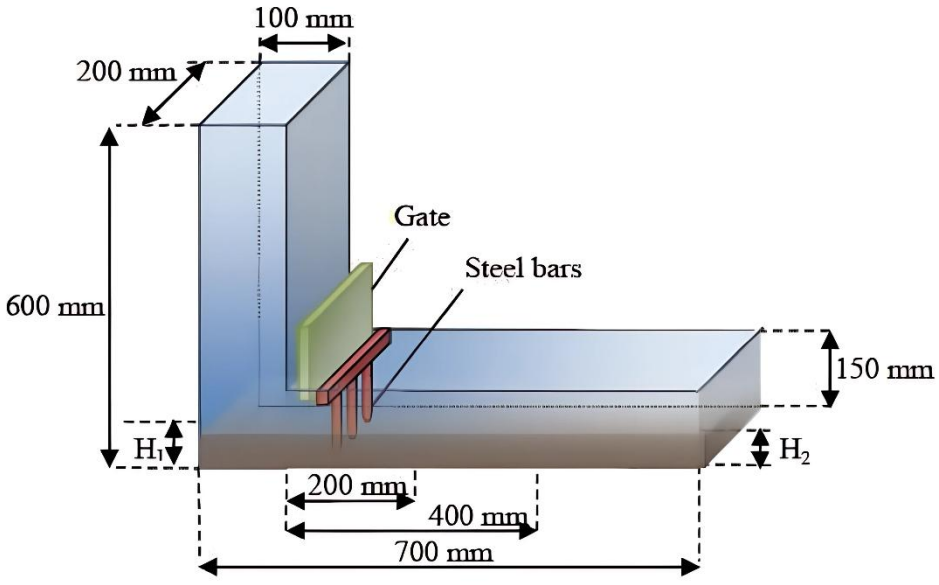

Figure 3: L-box test apparatus

The L-box may be represented with 2 or 3 smooth steel bars with a 12 mm diameter to indicate light or dense reinforcement, with distances between them of 59 mm and 41 mm, respectively. The L-box test is depicted in Plate 2. The acceptance criteria for the L-box test must adhere to the requirements given in BS EN 12350-10, 2010 [27].

- There is no evidence of segregation or bleeding.
- The passing ability ratio (PL) should fall within the range of 0.8 to 1.

Plate 2: L-box test of SCC

Calculate the passing ability ratio (PL) according to the Equation 2:

$$PL=H2/H1 \quad (2)$$

H1: the vertical part of the box's concrete depth, H2: The depth of the concrete at the terminus of the horizontal segment of the box.

2.3.3 V- funnel test

This test is utilized to assess the viscosity and filling capacity. The funnel is filled with concrete, and the gate is closed, necessitating approximately (0.012 m^3) of concrete for the entire filling process. A container is positioned below the funnel; the gate is then opened, and the duration of the concrete flow from the funnel is documented. The funnel test is illustrated in Figure 4 and Plate 3. The acceptance criteria for the V-funnel test must adhere to the requirements given in BS EN 12350-9, 2010 [28].

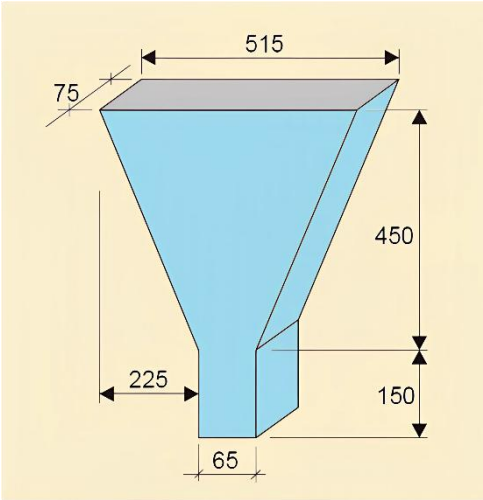

Figure 4: V-funnel test apparatus

Plate 3: V- funnel test of SCC

2.4 Concrete strain gauge

A concrete strain gauge measures the tensile strain of concrete at the lower section of the CFST beams.

2.5 LVDTs Location

One LVDT was situated under the beam's mid-span, while the other two were located beneath the applied load to assess the deflection.

2.6 Test setup

The tested beams were simply supported with a span of 1800 mm and subjected to four load points positioned at one-third intervals along the beam span, using AVERY hydraulic testing equipment with a capacity of 2500 kN at the University of Technology Civil Engineering structural laboratory. Plate 4 shows the specimen being examined.

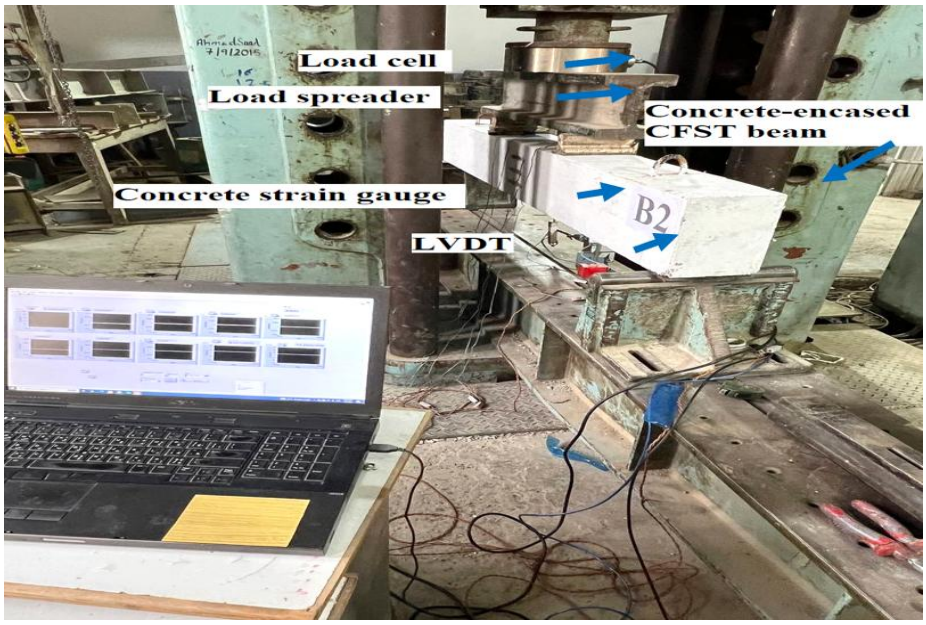

Plate 4: Testing apparatus and instrumentation for concrete-encased CFST beam

3. Results and discussion

The experimental investigation evaluated the influence of various parameters, including the presence of CFST on beam curvature, shear connection, cross-section size, steel tube ratio, compressive strength of outer concrete, compressive strength of concrete within filled steel tubes, steel fiber content, and unfilled steel tubes. Table 3 shows a comparison of the test results for the ultimate load and ultimate moment of the reference beam (B2) compared to beams (B1, B3, B4, B5, B6, B7, B8, and B9) using the variables that were studied. The relationship between the moment (M) and mid-span curvature (φ) in concrete-encased CFST beams. Each specimen exhibited elastic behavior during the initial loading stage, followed by a plastic response marked by a gradual decrease in stiffness until the maximum moment capacity was attained. The moment-curvature relationship for each beam will be analyzed, considering its specific variable. The results will subsequently be compared to the control beam B2, as depicted in Figure 5.

The theoretical calculation of the curvature at the midspan, as delineated by Han [29], is derived from the correlation between span length and deflection according to the Equation 3:

$$\varphi = \pi^2 . u_m / {L_e}^2 \quad (3)$$

where; φ: Curvature (1/m), u_m: Deflection at mid-span (m), L_e: Effective length span (m)

From Table 3 and Figure 5, it can be observed that the ultimate moment of the conventional beam (B1) is elevated by 141.9% in comparison to the concrete-encased CFST beam (B2). The curvature of the conventional beam (B1) is reduced by 30.4% in comparison to (B2). In a secondary variable analysis (shear connections), the ultimate moment is augmented by 12.96 percent when comparing beam (B3) to the reference beam (B2). Shear connections need sufficient space to convey shear forces and avert the separation of concrete and steel tubes. Shear connections improve the adhesion between concrete and steel tubes. The curvature of the beam is 14.6% less than that of beam B2. The research was undertaken to examine the impact of the cross-sectional dimensions of beam (B2), measuring 160×260 mm^2, in contrast to beam (B4), which measures 160×340 mm^2. The research indicates that increasing the section height from 260 mm to 340 mm leads to a 72.9% augmentation in the ultimate moment. Furthermore, the curvature of the beam diminishes by 34.8% in comparison to the beam (B2). The ultimate moment of the beam (B5) was augmented by 62.4% as a consequence of the increased quantity of steel tubes in concrete-encased CFST beams, leading to a more robust structural system. In comparison to beam B2, the beam curvature decreased by 11.3%. Enhancing the compressive strength of the outer concrete from 25 MPa (B2) to 45 MPa (B6) results in a 13.8% increase in the ultimate

moment relative to beam B2. The beam's curvature decreased by 19.03%. Increasing the compressive strength of the concrete inside the inner steel tubes makes a concrete-encased CFST beam stronger and better at supporting weight. When you look at the ultimate moment of beam (B2), which has a core compressive strength of 35 MPa, and beam (B7), which has a core compressive strength of 55 MPa, you can see that beam (B7) has a 6.7% higher ultimate moment. The curvature of the beam is 11.3% lower than that of the reference beam (B2). The ultimate moment of beam B8 decreases by 6.1% in the absence of steel fibers relative to the reference beam B2, which contains 1% steel fibers. The curvature decreased by 22.3%. The unfilled steel tubes for beam (B9) demonstrated a 13.97% reduction in the ultimate moment when compared to the reference beam (B2), which was constructed using 35 MPa self-compacted concrete. The curvature of the beam increased by 3.6%.

Initial cracks were observed at the yield moment (My), while the failure transpired at the ultimate moment (Mu). The initial cracks yielding were identified during the moments of yielding. 74.78, 31.22, 36.66, 56.54, 50.2, 34.97 k, 34.61, 28.69, and 24.98 kN.m correspond to mid-span curvatures of 0.0150 1/m, 0.0135 1/m, 0.0130 1/m, 0.0091 1/m, 0.0159 1/m, 0.0104 1/m, 0.0104 1/m, 0.0116 1/m, and 0.0105 1/m for B1, B2, B3, B4, B5, B6, B7, B8, and B9, respectively. The peak was detected at critical moments. The values recorded are 104.7 k, 43.3 , 48.9 , 74.8 , 70.3 , 49.3 , 46.1 , 40.6 k, and 37.2 kN.m, which correspond to mid-span curvatures of 0.048 1/m, 0.069 1/m, 0.059 1/m, 0.045 1/m, 0.061 1/m, 0.056 1/m, 0.061 1/m, 0.054 1/m, and 0.0714 1/m for B1, B2, B3, B4, B5, B6, B7, B8, and B9, respectively. The concrete strain gauge (S.G.) positioned at the bottom of the beam measures the tensile strain of concrete. Figure 6 illustrates that the conventional beam, the beam with a higher depth, and the beam with a higher ratio of CFST exhibit greater tensile strength than the other beams.

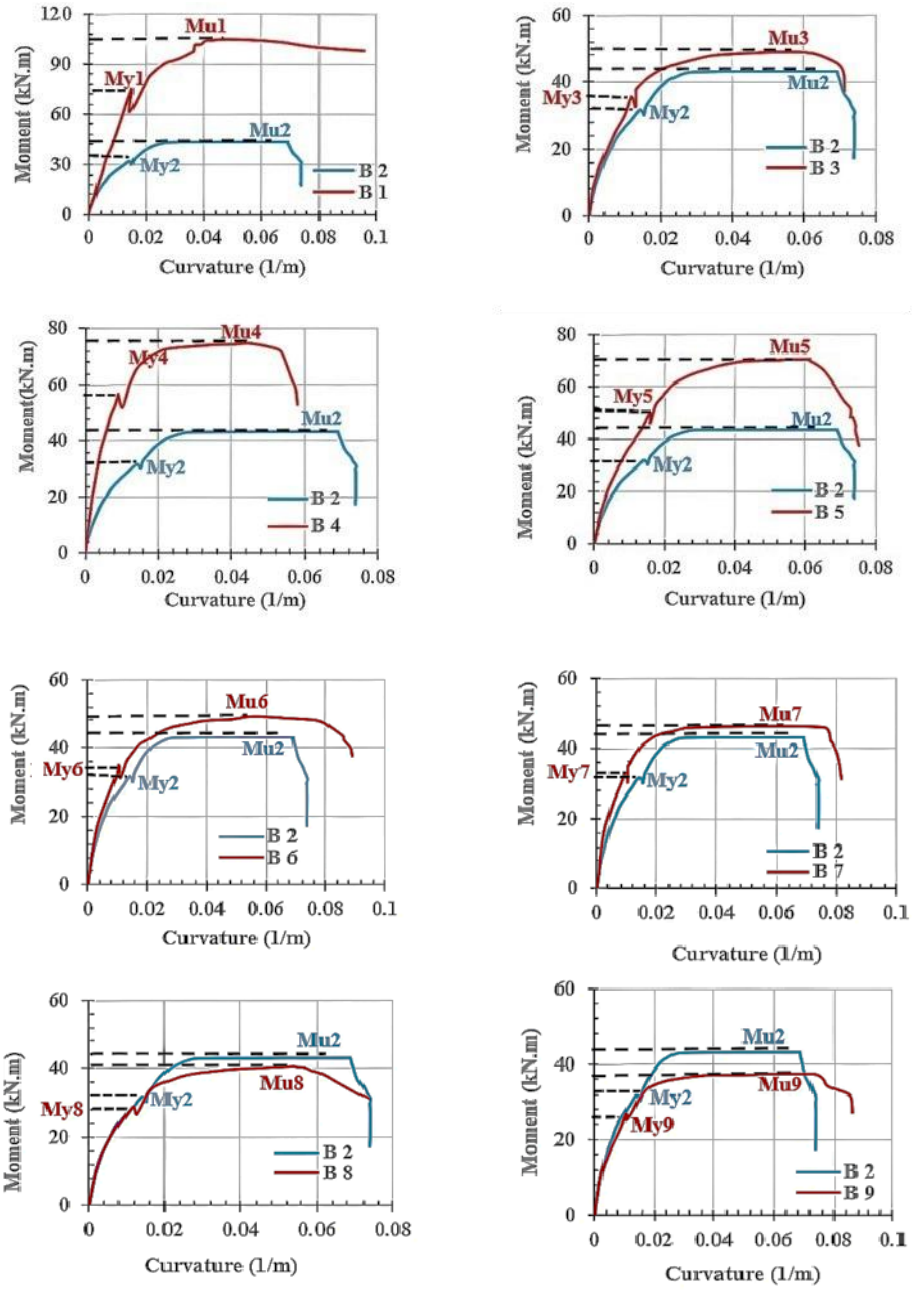

Figure 5: Moment-curvature relations of tested beams

Table 3: Information on experimental results for concrete-encased CFST beams

Specimens	Variables	Height of cross-section (H) (mm)	Percentage of volume of steel fiber	Compressive strength of outer concrete fc (MPa)	Compressive strength of concrete in FST fc (MPa)	Shear connector (mm)	CFST %	Maximum load (P_u) kN	Maximum moment (Mu) kN.m	Mid-span deflection (mm)	Curvature (1/m)
B1	Conventional	260	1	25	---	---	---	337.7	104.7	17.2	0.048
B2	Reference	260	1	25	35	---	2. 7	139.6	43.3	24.7	0.069
B3	Shear connector	260	1	25	35	75	2.7	157.7	48.9	21.1	0.059
B4	Cross-section size	340	1	25	35	---	2.7	241.4	74.8	16.1	0.045
B5	Ratio of CFST	260	1	25	35	---	5.4	226.7	70.3	21.9	0.0612
B6	Compressive strength of outer concrete	260	1	45	35	---	2.7	158.9	49.3	20.0	0.056
B7	Compressive strength of concrete in FST	260	1	25	55	---	2.7	148.9	46.1	21.9	0.0612
B8	Steel fiber content	260	0	25	35	---	2.7	131.1	40.6	19.2	0.054
B9	Unfilled steel tube	260	1	25	---	---	2.7	120.1	37.2	25.6	0.0715

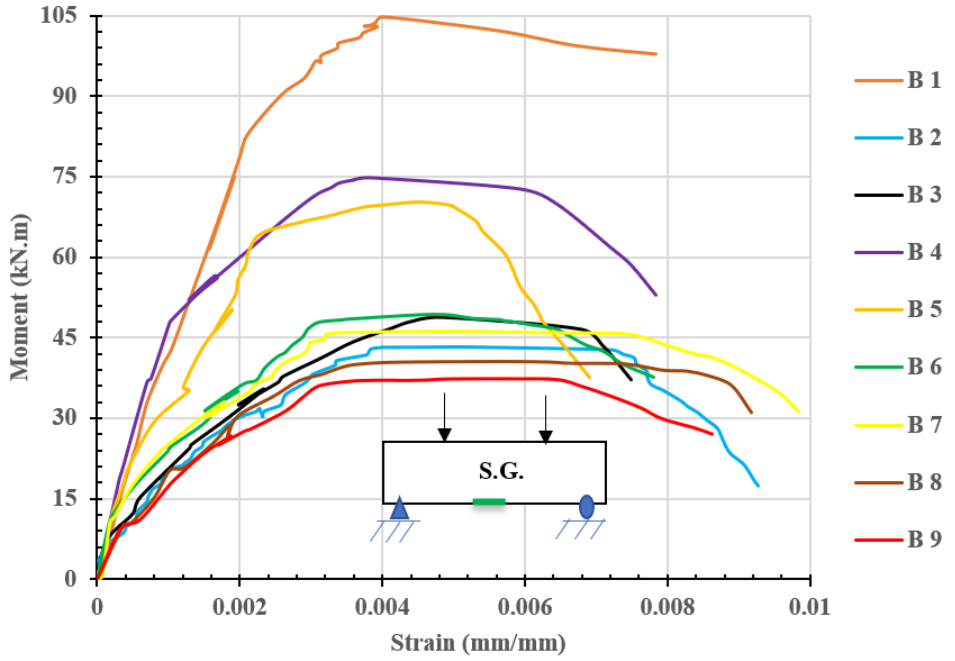

Figure 6: Moment-strain behavior for strain gauge in the tested beams

4. Failure modes of tested beams

Plate 5 presents the failure modes observed in the examined beam specimens. Flexural fractures arise in regions subjected to pure bending. The nine beams exhibited conventional flexural failure, marked by concrete crushing at the mid-span of the beam. The failure takes place at the peak moment in the mid-span. Strain gauges quantify the compressive strain of concrete precisely at the load application site during testing. The specimens exhibit a peak concrete compressive strain at failure between 0.00233 and 0.00450.

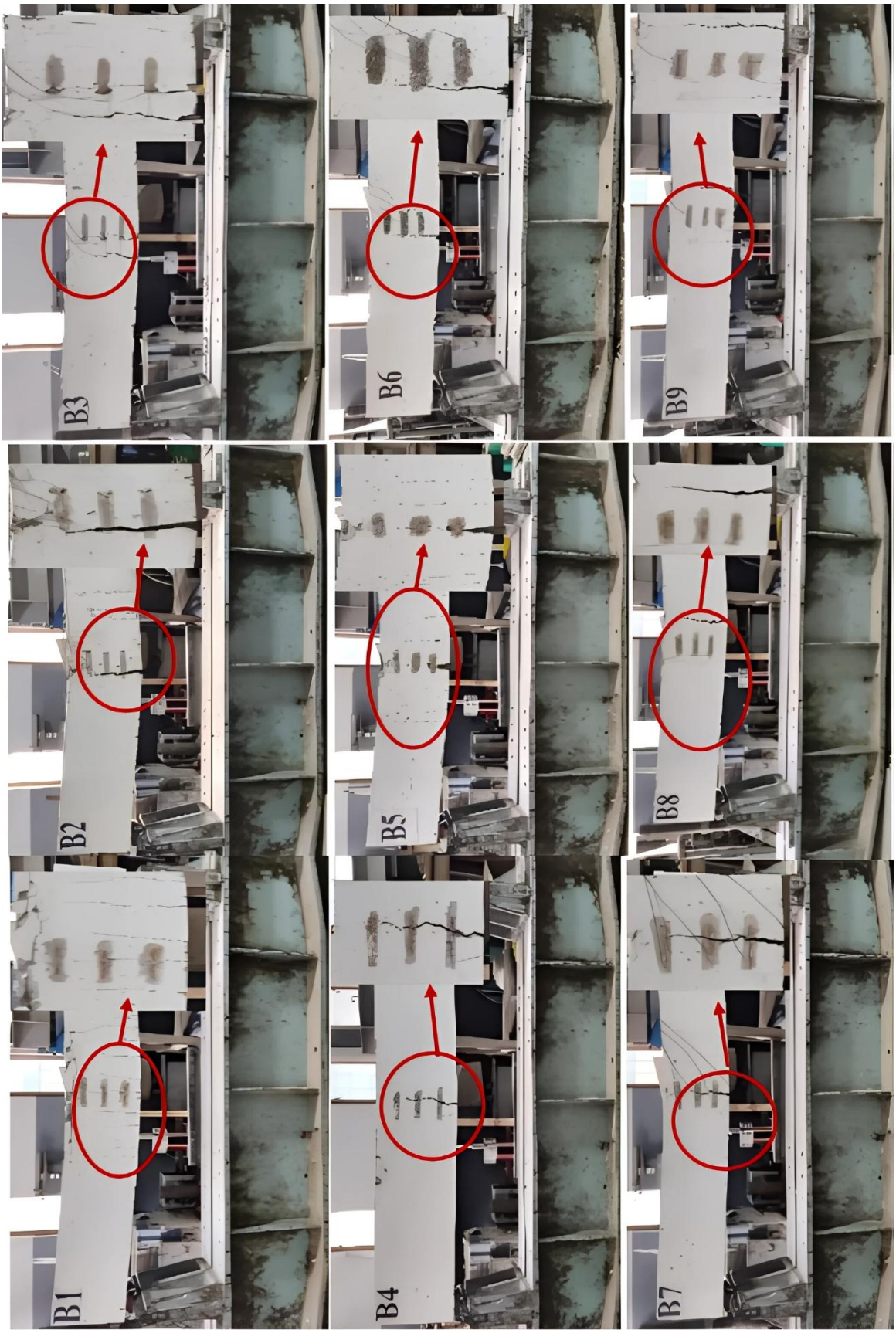

Plate 5: Modes of failure of tested beams

The modes of failure are compatible with the work of Chen et al. [10]. The failure mechanisms of the conventional beam B1, reinforced with 25 mm diameter bars, and beam B5, reinforced with 25 mm diameter steel tubes at 5.4%, are similar. The uniform distribution of flexural fractures occurs throughout the pure flexural zone. Cracks initially formed and progressed in the area, signifying pure bending. With increasing load, numerous flexural cracks were observed in both the central and shear regions. Cracks in the bending region quickly extended to approximately 60% of the beam's depth. Control beam B2 demonstrates flexural cracking in the pure bending region at mid-span as the load escalates. The failure mechanism triggers the formation of a vertical crack that extends upward within the beam, progressing toward the compression zone. The remaining beam specimens (B3, B4, B6, B7, B8, and B9) exhibit flexural failure upon loading, resulting in a hairline fracture in the tension zone beneath the mid-span. As the load increases, the crack propagates and extends into the compression zone, exhibiting minor variations in width and length based on beam parameters.

5. Conclusion

The ultimate moment and curvature of CFST beam were 41% and 328.95% of that conventional beam. The peak moment of the concrete-encased CFST beam increased by 12.96, 72.9, 62.4, 13.8, and 6.7% while the curvature reduced by 14.6, 25.9, 11.3, 19.03, and 11.3% compared to the reference beam due to shear connectors, increasing section height from 260 to 340 mm, increasing CFST ratio from 2.7% to 5,4%, increasing outer concrete compressive strength from 25 to 45 MPa, and increasing core concrete compressive strength from 35 to 55 MPa respectively. Increasing the steel fiber content in concrete beams leads to improvements in toughness, ductility, and flexural strength. This enhancement positively affects the moment-curvature relationship by increasing load-carrying capacity and regulating crack behavior, in addition to improving energy absorption characteristics. The enhancement of compressive strength significantly influences the moment-curvature behavior of concrete due to the increase of fracture energy of specimens. The peak moment of the concrete-encased CFST beam decreased by 6.1% and 13.97%, while the curvature reduced by 22.3% and increased by 3.6% compared to the reference beam due to the absence of steel fiber in outer concrete and unfilled steel tubes with self-compacted concrete.

Author contributions

Conceptualization, **R. Abdulkhudhur**, **H. Al-Quraishi**, and **M. Elwi**; data curation, **R. Abdulkhudhur**, and **H. Al-Quraishi**; formal analysis, **R. Abdulkhudhur**, and **M. Elwi**; investigation, **R. Abdulkhudhur**, and **H. Al-Quraishi**; methodology, **R. Abdulkhudhur**, and **H. Al-Quraishi**; project administration, **H. Al-Quraishi**; resources, **R. Abdulkhudhur**, **M. Elwi**; software, **R. Abdulkhudhur**; supervision, **H. Al-Quraishi**, **M. Elwi**; validation, **R. Abdulkhudhur**, **H. Al-Quraishi**, and **M. Elwi**; visualization, **R. Abdulkhudhur**, and **H. Al-Quraishi**; writing—original draft preparation, **R. Abdulkhudhur**; writing—review and editing, **H. Al-Quraishi**, and **M. Elwi** All authors have read and agreed to the published version of the manuscript.

Funding

This research received no specific grant from any funding agency in the public, commercial, or not-for-profit sectors.

Data availability statement

The data that support the findings of this study are available on request from the corresponding author.

Conflicts of interest

The authors declare that there is no conflict of interest.

References

[1] L.- H. Han and Y. – F. An., Performance of concrete-encased CFST stub columns under axial compression, J. Constr. Steel Res., 93 (2014) 62–76. https://doi.org/10.1016/j.jcsr.2013.10.019

[2] R. Abdulkhudhur, H. Al-Quraishi, M. Elwi, Numerical analysis of concrete-encased concrete filled steel tube beams, AIP Conf. Proc., 3219 (2024) 020049. https://doi.org/10.1063/5.0236329

[3] H. Al-Quraishi, M. Al-Farttoosi, R. Abdulkhudhur, Tension Lap Splice Length of Reinforcing Bars Embedded in Reactive Powder Concrete (RPC), Structures, 19 (2019) 362–368.

[4] Y.-F. An and L.-H. Han, Behaviour of concrete-encased CFST columns under combined compression and bending, J. Constr. Steel Res., 101 (2014) 314–30. https://doi.org/10.1016/j.jcsr.2014.06.002

[5] R. Abdulkhudhur, H. Al-Quraishi, O. H. Abdullah, Effect of steel fiber on the shear transfer strength across a crack in reactive powder concrete, IOP Conf. Ser. Mater. Sci. Eng., 737 (2020) 012001. https://doi.org/10.1088/1757-899X/737/1/012001

[6] R. Abdulkhudhur, H. Al-Quraishi, M. Elwi, Numerical analysis of concrete-encased concrete filled steel tube columns, AIP Conf. Proc., 3219, 2024, 020050. https://doi.org/10.1063/5.0236331

[7] H. Al-Quraishi, R. Abdulkhudhur, A. Abdulazeez, Shear Strength Behavior of Fiber Reinforced Recycled Aggregate Concrete Beams, Int. Rev. Civ. Eng., 12 (2021) 314. http://dx.doi.org/10.15866/irece.v12i5.19972

[8] Y.-F. An, L.-H. Han and C. Roeder, Flexural performance of concrete-encased concrete-filled steel tubes, Mag. Concr. Res., 66 (2014) 249–267. http://dx.doi.org/10.1680/macr.13.00268.

[9] L.-H. Han, Y-F. An, C. Roeder and Q-X. Ren, Performance of concrete-encased CFST box members under bending, J. Constr. Steel Res., 106 (2015) 138–153. https://doi.org/10.1016/j.jcsr.2014.12.011

[10] J-Y. Chen, F-C. Wang, L-H. Han and T-M. Mu, Flexural performance of concrete-encased CFST box members, Structures, 27 (2020) 2034–2047. http://dx.doi.org/10.1016/j.istruc.2020.07.065

[11] R. Montuori and V. Piluso, Analysis and modeling of CFT members: Moment curvature analysis, Thin-Walled Struct., 86 (2015) 157–166. https://doi.org/10.1016/j.tws.2014.10.010

[12] G. Li, D. Liu, Z. Yang and C. Zhang, Flexural behavior of high strength concrete filled high strength square steel tube, J. Constr. Steel Res., 128 (2017) 732–744. http://dx.doi.org/10.1016/j.jcsr.2016.10.007

[13] C-C. Hou, L-H. Han, F-C. Wang and C-M. Hu, Study on the impact behaviour of concrete-encased CFST box members, Eng. Struct., 198 (2019) 109536. https://doi.org/10.1016/j.engstruct.2019.109536

[14] J-Y. Chen, F-C. Wang, L-H. Han and T-M. Mu, Flexural performance of concrete-encased CFST box members, Structures, 27 (2020) 2034–2047. https://doi.org/10.1016/j.istruc.2020.07.065

[15] A.W. Al Zand, W.H.W. Badaruzzaman and W.M. Tawfeeq, New empirical methods for predicting flexural capacity and stiffness of CFST beam, J. Constr. Steel Res., 164 (2020) 105778. http://dx.doi.org/10.1016/j.jcsr.2019.105778

[16] A. W. Al Zand, M. M. Ali, R. Al-Ameri, W. H. W. Badaruzzaman, W.M. Tawfeeq, E. Hosseinpour and Z. M. Yaseen, Flexural Strength of Internally Stiffened Tubular Steel Beam Filled with Recycled Concrete Materials, Materials, 14 (2021) 6334. https://doi.org/10.3390/ma14216334

[17] S. Liu, Z. Ji, S. Li, X. Li, Y. Liu, and S. Zhao, Bending Test of Rectangular High-Strength Steel Fiber-Reinforced Concrete-Filled Steel Tubular Beams with Stiffeners, Buildings, 14 (2024) 3678. https://doi.org/10.3390/buildings14113678

[18] J. M. Suthar, U. K. Koshti, S. P. Purohit, and H. J. Jadeja, Moment Curvature of Reinforced Concrete beams- An analytical and experimental validation, ASPS Conference Proceedings, 2022, 619-623. http://dx.doi.org/10.38208/acp.v1.557

[19] S. Dhakal, and M. A. Moustafa, MC-BAM: Moment–curvature analysis for beams with advanced materials, Software, 9 (2019) 175–182. https://doi.org/10.1016/j.softx.2019.01.014

[20] H. Al-Thairy, Analytical predictions of moment curvature relationship of steel beam-columns under fire attack, MATEC Web of Conferences, 162 (2018) 04006. https://doi.org/10.1051/matecconf/201816204006.

[21] D. Fa-xing and Y.U. Zhi-wu, Pure bending properties of self-compacting concrete filled circular steel tube, J. Traffic Transp. Eng., 6 (2006) 63–68.

[22] H. Wu, C. Wang, Y. Bai, S. Tong, and Y. Liu, Experimental study on rubber concrete filled steel tube members under pure bending, Sci. Rep., 12 (2022) 9385. https://doi.org/10.1038/s41598-022-13659-3.

[23] Z. Rahmani, M. Naghipour and M. Nematzadeh, Flexural Performance of High-strength Prestressed Concrete-encased Concrete-filled Steel Tube Sections, Int. J. Eng. Trans. C: Aspects, 32 (2019) 1238–1247. https://doi.org/10.5829/ije.2019.32.09c.03

[24] A. Hamoda, S. Fayed, W. Mansour and M. Emara, Behavior of Reinforced Concrete Circular Columns Subjected to Double Curvature Buckling Moment, Int. J. Concr. Struct. Mater., 18 (2024). http://dx.doi.org/10.1186/s40069-024-00712-w

[25] EFNARC, S., 2002. Specification and guidelines for self-compacting concrete, London, UK: Association House, 32, p.34.

[26] BS EN, 12350-8: 2010. Testing fresh concrete - Part 8: Self-compacting concrete -Slump-flow test, British Standards Institute, London, United Kingdom.

[27] BS EN, 12350-10: 2010. Testing fresh concrete - Part 10: Self-compacting concrete – L box test, British Standards Institute, London, United Kingdom.

[28] BS EN, 12350-9: 2010. Testing fresh concrete - Part 9: Self-compacting concrete -V-funnel test, British Standards Institute, London, United Kingdom.

[29] L-H. Han, Flexural behaviour of concrete-filled steel tubes, J. Constr. Steel Res., 60 (2004) 313–337. https://doi.org/10.1016/j.jcsr.2003.08.009